Title
Effect of Green Density on Densification and Creep During Sintering

Authors
Rahaman, M.N.
Jonghe, L.C. De
Chu, M.-Y.

Publication Date
1990-05-01

LBL-29085
Preprint

Lawrence Berkeley Laboratory
UNIVERSITY OF CALIFORNIA

Materials & Chemical Sciences Division

Submitted to Journal of the American Ceramic Society

Effect of Green Density on Densification and Creep During Sintering

M.N. Rahaman, L.C. De Jonghe and M.–Y. Chu

May 1990

Prepared for the U.S. Department of Energy under Contract Number DE-AC03-76SF00098.

DISCLAIMER

EFFECT OF GREEN DENSITY ON DENSIFICATION AND CREEP DURING SINTERING

Mohamed N. Rahaman*

University of Missouri-Rolla, Ceramic Engineering Department
Rolla, Missouri 65401

Lutgard C. De Jonghe* and May-Ying Chu*

Lawrence Berkeley Laboratory, Materials and Chemical Sciences Division, and
Department of Materials Science and Mineral Engineering,
University of California, Berkeley, California 94720

Abstract

The effect of green density on both the densification rate and the creep rate was measured simultaneously during sintering by loading dilatometry. The experiments were performed on zinc oxide powder compacts with five different green densities covering a range of 0.39 to 0.73 of theoretical. The samples were heated at a constant rate of 4°C/min up to 1100°C in air. The densification rate at any temperature increases significantly with decreasing green density. The data for the densification rate and creep rate as a function of density show two quite distinct regimes of behavior; the rates were strongly dependent on density below 0.80 while above this value they were weakly dependent on density. The ratio of the densification rate to the creep rate was almost independent of temperature but increased almost linearly with increasing green density. The representation of the data in terms of models for sintering and creep is discussed.

Supported by the Division of Materials Sciences, Office of Basic Energy Sciences, U. S. Department of Energy, under Contract No. DE-AC03-76SF00098.

---

* Member, the American Ceramic Society.

I. Introduction

The sintering of heterogeneous or constrained powder compacts involves a combination of volumetric densification and creep (or shear) deformation. Differential densification between different regions of the body leads to the generation of transient stresses which, if not relieved by creep processes, can severely limit the overall densification rate. It is therefore important to understand not only the densification and creep processes separately, but also their interaction.

The technique for studying densification, creep, and their interaction was developed by De Jonghe and Rahaman[1-3] and is usually referred to as loading dilatometry. In this technique, a controlled, uniaxial stress is applied during sintering; determination of the time dependent axial and radial strains allows the separation of the volumetric strain and the creep strain. A feature of the work of Rahaman and De Jonghe is that the hydrostatic component of the applied uniaxial stress is low compared to the sintering stress produced by interface tensions. Because of this, the densification mechanism for the loaded sample is the same as that for freely sintered sample. In work performed later, Venkatachari[4] and Raj used considerably higher uniaxial stresses to study the interaction between deformation and densification; the work of Venkatachari and Raj would therefore be more appropriate to sinter-forging.

In the series of studies, De Jonghe and co-workers[5-7] have established a basic understanding of the interaction between creep and densification and their dependence on material and processing variables. In the context of the present paper, the parameter that is most appropriate for quantifying this interaction is the ratio of the densification rate to the creep rate, denoted as $\dot{\varepsilon}_\rho/\dot{\varepsilon}_c$. This ratio has been shown to be almost independent of temperature and heating rate[6] and of sintered density[5] over a wide range covering the early and intermediate stage of sintering. The ratio is, however, system specific[7]; for example, it is much higher for polycrystalline bodies compared to glasses of the same particle size. The present paper deals with the effect of the green density on the densification and creep during sintering. Green density is a primary parameter that is normally used to characterize a sample prior to sintering.

A number of studies has examined the effect of green density on densification. Bruch[8] found that the densification rate of Al_2O_3, measured in the intermediate and final stages of isothermal sintering, was strongly dependent on the green density but that the grain growth rate was independent of green density. At

any temperature, the porosity, P, of the sample after sintering for time, t, could be described by the relation $P = Ct^{-n}$, where C and n are constants. Bruch described the densification rate as retarded or "subnormal" if n was less than 0.4 and as "normal" if n was equal to 0.4. Thus, at any temperature there was a green density below which or above which the sintering was "subnormal" or "normal" respectively. Even in the "normal" sintering range, the densification rate was still strongly dependent on the green density, decreasing with increasing green density.

Greskovich[9] studied the initial stage sintering kinetics of an agglomerated aluminum oxide powder during isothermal sintering at 1270 and 1370°C and found almost no difference in the shrinkage rate for green densities between 0.42 and 0.50; however, the shrinkage rate decreased as the green density decreased from 0.40 to 0.31. Woolfrey[10] examined the initial stage sintering kinetics of UO_2 in both isothermal heating and constant heating rate experiments. Under isothermal conditions, Woolfrey's observations were somewhat similar to those of Greskovich; it was found that the shrinkage rate at a fixed shrinkage (2%) was nearly the same for green densities of 0.40 and 0.50 but decreased with decreasing green density below 0.40. In addition, for the constant heating rate experiments, the shrinkage rate at a fixed temperature (1000°C) showed a similar trend with green density.

Occhionero and Halloran[11] found that the shrinkage rate of Al_2O_3, measured in the range of 1 to 10% shrinkage during isothermal sintering, was independent of green density for green densities between 0.49 and 0.55. However, the pore size distribution during sintering and the density at which grain growth commenced were affected by the green density. From a comparison of their data with a model put forward by Yan, Cannon, and Chowdhry[12] for microstructure evolution in which grain growth and densification occur simultaneously, Occhionero and Halloran concluded that increasing green density delayed the onset of grain growth.

The work reported in the present paper constituted a study into the effect of green density in the rage of 0.39 to 0.73 on the densification and creep kinetics of ZnO. To acquire the data from the earliest stages of sintering under carefully controlled conditions, the experiments were performed at a constant heating rate (of 4°C/min up to 1100°C) rather than isothermally.

II. Experimental Procedure

Zinc oxide powder* compacts (≈ 6 mm in diameter by 6 mm) with five different green densities in the range 0.39 to 0.73 of theoretical were prepared. Samples with green densities of 0.39 and 0.51 were formed by uniaxial compression of the powder in a die, while sample green densities of 0.59, 0.66, and 0.73 were prepared by further compacting the die pressed samples (green density 0.51) in a cold isostatic press. Each green density value was obtained to within ± 0.01 by this procedure.

Constant heating rate sintering was performed in a loading dilatometer[1] with an applied load or without load ("free" sintering). The samples were sintered in air under identical temperature profiles from room temperature to 1100°C at 4°C/min. For each green density, a sample was free-sintered, after which another sample was sintered under an initial applied stress of 0.22 MPa. The repeatability of the axial shrinkage data was checked by performing additional runs with or without applied load for the sample with green density of 0.51. The mass, length and diameter of the sintered samples were measured at the end of each experiment. Further, to check the anisotropy of the shrinkage under load against earlier work, samples with green density of 0.51 were sintered under an applied stress of 0.22 MPa up to fixed temperatures between 500°C and 1000°C, quickly removed from the dilatometer, and finally their length and diameter were measured. The microstructure of selected samples was observed by scanning electron microscopy of fracture surface.

III. Results

The axial strain, ε_z, versus temperature, T, for samples with green densities of 0.39, 0.59, and 0.73 that were sintered either freely or with an applied uniaxial stress is shown in Fig. 1. The data for the other green densities (0.51 and 0.66) have been omitted to maintain the clarity of this figure. The ε_z values were reproducible to within ± 0.01 at any temperature.

The shrinkage of the free-sintered samples is nearly isotropic; however, the loaded samples shrink anisotropically because of the creep deformation caused by the imposed uniaxial stress. The data for ε_z versus the radial strain, ε_r, measured at the end of each experiment, is shown in Fig. 2 for the samples sintered under the

*Reagent grade, Mallinckrodt Inc., Paris, Kentucky.

applied stress. The data for a green density of 0.44 of theoretical obtained in earlier work[6] performed under the same conditions are also shown in Fig. 2. The earlier work had shown that ε_z was approximately proportional to ε_r, and this relationship was also observed in the present work for the sample with green density of 0.51. In the present data analysis, the proportionality between ε_z and ε_r was therefore assumed for each green density.

The density, ρ, calculated from the ε_z data for the free-sintered samples is shown as a function of time in Fig. 3. All of the curves have the well-observed sigmoidal shape and the final sintered densities are larger than 0.96 of theoretical even for the sample with the lowest green density of 0.39. The results therefore indicate that there is no intrinsic barrier to achieving high sintered densities even for green densities as low as 0.39.

The volumetric densification strain rate, $\dot{\varepsilon}_\rho$, defined as $(1/\rho)\, d\rho/dt$, was calculated from the data of Fig. 3 by fitting smooth curves to the data and differentiating. The results are shown in Fig. 4 as a function of T. $\dot{\varepsilon}_\rho$ is strongly dependent on the green density over most of the temperature range except for a small region between 725°C and 750°C over which it is weakly dependent. Figure 5 shows the data for $\dot{\varepsilon}_\rho$ as a function of the sintered density, ρ. A striking feature of this plot is the strong dependence of $\dot{\varepsilon}_\rho$ on green density for ρ values below ≈ 0.80 and the weak dependence above this value.

The creep strain $\dot{\varepsilon}_c$ was calculated from the data of Figs. 1 and 2 and the creep strain rate, $\dot{\varepsilon}_c$ at a constant, normalized stress of 0.20 MPa was found by a previously outlined procedure[3,6]. Figure 6 shows the data for $\dot{\varepsilon}_c$ as a function of ρ. Trends similar to those of the densification rate data of Fig. 5 are observed. The similarity of the densification and creep curves reinforces an earlier analysis[3] in which both processes were considered to be controlled by the same mass transport mechanism.

An appropriate parameter for characterizing the simultaneous creep and densification behavior during sintering is the ratio of the densification rate to the creep rate, i.e., $\dot{\varepsilon}_\rho/\dot{\varepsilon}_c$, at a fixed, normalized, applied stress. Figure 7 shows this ratio, normalized to an applied uniaxial stress of 0.20 MPa, as a function of temperature, T. It is seen that $\dot{\varepsilon}_\rho/\dot{\varepsilon}_c$ for any green density is relatively constant with T, but at a fixed value of T, it increases with increasing green density.

Figure 8 shows scanning electron micrographs of the fracture surfaces for samples with green densities of 0.39 (sample A), 0.51 (sample B), and 0.73 (sample C) that were free sintered to 1100°C and then cooled. The sintered densities of the samples were nearly identical (≈ 0.97 of the theoretical). The grain size and fracture

mode of samples B and C are nearly identical. However, there is a subtle difference in the porosity distribution; sample C has somewhat more porosity along the grain edges compared to sample B. The fracture surface of sample A shows more extensive trans-granular fracture compared to samples B and C.

IV. Discussion

It is clear from Fig. 4 that green density has a significant effect on the densification rate at any temperature. The magnitude of this effect, however, varies with temperature. The densification rate is a strong function of the green density below ≈ 675°C and above ≈ 775°C; between these two temperatures (where the densification rate is nearly at its maximum), green density has a smaller effect. The effect of green density on the grain size of the sintered samples is relatively insignificant for green densities between 0.51 and 0.73, as seen from Fig. 8.

As summarized earlier, a number of workers found no effect of green density on the (initial stage) densification rate during isothermal sintering of other powders for the green density range of 0.40 - 0.50 (Greskovich[9], Woolfrey[10]) and 0.49 - 0.55 (Occhionero and Halloran[11]). Woolfrey[10] also found no effect of green density during constant heating rate sintering for the green density range of 0.40 - 0.50. A possible reason why these workers observed no effect of green density is the rather limited range of green densities studied. For example, the present data show that below 800°C, the densification rate is reduced by a factor of 1.2 - 1.4 in going from a green density of 0.39 to 0.51. Densification rate differences of this order can be difficult to detect reliably unless the experimental variables are well controlled.

The data of Fig. 5 show that green density has a very strong effect on the densification rate for sintered densities < 0.80 but a relatively weak effect above this sintered density. They indicate that the microstructure development in this powder progresses towards normalization at some fixed value of the sintered density (≈ 0.80 for the range of green densities used). Therefore, apart from a change of scale, the microstructures at this value of the sintered density should be almost the same. As shown in Fig. 9, this is indeed observed for samples with green densities of 0.39 and 0.73 that have been sintered to a density of 0.81 ± 0.01. Once this normalization has occurred, the samples should densify to the same final density, as is observed (Fig. 3).

Rahaman and De Jonghe[5] showed that the densification rate of the same ZnO powder under isothermal conditions followed a relationship of the form:

$$\dot{\varepsilon}_\rho = \frac{AD\Sigma\phi^{\frac{n+1}{2}}}{X^n kT} \qquad (1)$$

where A is a geometrical constant, D is the volume diffusion coefficient, Σ is the sintering stress[7] (defined as an equivalent external stress leading to the same densification rate as from the interface tension forces), ϕ is a function of density which relates the internal grain boundary area to the external area of the powder compact (ϕ is usually referred to as the stress intensification factor),[7,13,14] X is the mean interpore distance, k is the Boltzmann constant, T is the absolute temperature, and n is an exponent which depends on the mechanism of densification (i.e., n = 2 for volume diffusion[15,16] and n = 3 for grain boundary diffusion[17]). It would be instructive to determine how well Eqn. (1) can account for the present data for constant heating rate sintering.

A first step is to relate the initial pore spacing, X_o, to the green density, ρ_o. For this, a microstructural model must be assumed. While, in general, a wide range of structures could accommodate a lowering of the green density at constant particle size, two idealized extremes may be recognized readily: a structure consisting of an invariant matrix into which an increasing volume fraction of larger heteropores are mixed; or, a structure in which the existing porosity is uniformly dilated. A two-dimensional equivalent of the latter would be an interconnected ring structure of particles in which the pore coordination number increases with decreasing density. Such a structure would lead to a mean pore spacing that can be related to the overall density when considering the total sample volume V to consist of a fixed number, N, of pores and a fixed volume of solids, Vs. Then $X^3_o = V/N = K\,\rho^{-1}_o$, where K is a constant. For now, this model is assumed, so that, at a fixed temperature, and in the early stages of sintering when $X \approx X_o$, Eqn. 1 would give, with n=2 for volume diffusion control[5]

$$\Sigma \approx \frac{B\,\dot{\varepsilon}_\rho \rho^{\frac{2}{3}}}{\phi^{\frac{3}{2}}} \qquad (2)$$

where B is a constant. For the same ZnO, ϕ has been determined from isothermal creep-sintering experiments and can be described by

$$\phi \cong \exp[a(1-\rho)] \tag{3}$$

where a ≈ 5. Given the present assumption, and using Eqns. (2) and (3) and the data of Figs. 3 and 4, Σ as a function of ρ_o at T = 650° can be obtained from the densification strain rates only.

The resulting values of Σ can be compared for self-consistency with those obtained from the ratio of $\dot{\varepsilon}_\rho/\dot{\varepsilon}_C$ the densification rate over the creep rate. For the present low-stress creep experiments, the creep mechanism would be expected to the same as the densification mechanism[3]. Following Eqn. (1), the creep rate, $\dot{\varepsilon}_C$ can be expressed by the equation:

$$\dot{\varepsilon}_c = \frac{CD\,\sigma_z \phi^{\frac{n+1}{2}}}{X^n kT} \tag{4}$$

where C is a geometrical constant and σ_Z is the applied uniaxial stress. The ratio of the densification rate to the creep rate is then:

$$\frac{\dot{\varepsilon}_\rho}{\dot{\varepsilon}_c} = \frac{F\Sigma}{\sigma_z} \tag{5}$$

where F is a constant.

The comparison between the values for Σ found directly from Eqn. (2) and those from Eqn. (5) is shown in Fig. 10; the constants have been chosen such that coincidence of the data is forced at ρ_o = .51. The two different paths to $\Sigma(\rho_o)$ appear to agree well, to within an unknown constant. Both these analyses then lead to a sintering stress that depends, empirically, on the green density at constant particle size in the following manner:

$$\Sigma = \Sigma_o(g\,\rho_o - 1) \tag{6}$$

It is tempting to relate Σ_o to the initial particle size and to relate Eqn. (6) to the concepts modeled by Kellett and Lange regarding the sintering of rings of particles.[18] Generally, one must then expect the sintering stress to be proportional to the inverse of the particle size, and to a function that decreases with increasing pore

coordination number. This, however, would leave unanswered the reason for the observed constancy of Σ as densification proceeds, and a further analysis will require additional, parametric experimental work.

The functional form of X^n (where X is the mean interpore distance) versus sintered density (or temperature) can also be computed. According to Eqn. (1), and putting

$$D = D_o \exp\left(\frac{-Q_d}{kT}\right) \tag{7}$$

where D_O is a constant, and Q_d is the activation energy for the densification process:

$$X^n = \frac{H \Sigma \phi^{\frac{3}{2}} \exp\left(\frac{-Q_d}{kT}\right)}{kT \dot{\varepsilon}_p} \tag{8}$$

where H is a constant. Using Q_d = 50 Kcal/mole[19,20]; Eqns. (3) and (4) and the data of figs. 3 and 4, the results for X^n versus T_O are shown in Fig. 11 for green densities between 0.39 and 0.73.

The calculated values of X^n can be represented by,

$$X^n = \frac{X'^n(T)}{\rho_o^{\frac{2}{3}}} \tag{9}$$

where the factor $\rho_o^{-2/3}$ originates in the assumptions that led Eqn. (2), and where $X'^n(T)$ is not a function of sintered density up to some point where a significantly stronger temperature or a sintered density dependence sets in. The onset of this stronger temperature or density dependence can be correlated with a value of the sintered density of about 90% of theoretical. It may be conjectured that this onset of rapid coarsening coincides with reaching closed porosity when lower activation energy processes, such as surface diffusion, can no longer operate. These findings and considerations are in agreement with an earlier study on coarsening and densification in zinc oxide by Chu et al (20). While direct confirmation from extensive microstructural examination are needed to establish fully the validity of the behavior of the interpore spacing during coarsening, the current findings

indicate an evolution and pore behavior during sintering that is also reflected in the recent neutron scattering work of Long et al[21] that indicates a constant pore size during densification, only dependent on green density, up to the point where closed porosity is reached and rapid pore coarsening is observed.

V. Conclusions

For these experiments in which ZnO powder compacts with green densities of 0.39 to 0.73 were sintered with or without an applied uniaxial load and at a constant heating rate of 4°C/min up to 1100°C, it was found that the densification rate and the creep rate were affected significantly by the green density. The densification rate at any temperature increased with decreasing green density.

The data for the densification rate and the creep rate as a function of sintered density showed two distinct regimes of behavior; the rates were strongly dependent on green density for sintered densities below ≈ 0.80, while above this value they were weakly dependent on the green density. This could be understood in terms of a normalization of the microstructure during the sintering process.

The sintering stress increases approximately linearly with green density for the range of green densities used in this work. This increase in the sintering stress accounts for the observed linear increase in the ratio of the densification rate to the constant stress creep rate as a function of green density.

For sintered densities of up to 0.92, the mean interpore distance (which is used to represent the microstructural coarsening) is a function of temperature (or time) only, and is independent of sintered density. Above this density value, it is a strong function of sintered density and/or temperature.

References

1. L. C. De Jonghe and M. N. Rahaman, *"A Loading Dilatometer,"* Rev. Sci. Instrum., **55** [12] 2007-2010 (1984).

2. M. N. Rahaman and L. C. De Jonghe, *"Sintering of CdO Under Low Applied Stress,"* J. Am. Ceram. Soc., **67** [10] C-205–C207 (1984).

3. M. N. Rahaman, L. C. De Jonghe, and R. J. Brook, *"Effect of Shear Stress on Sintering,"* J. Am. Ceram. Soc., **69** [1] 53-58 (1986).

4. K. R. Venkatachari and R. Raj, *"Shear Deformation and Densification of Powder Compacts,"* J. Am. Ceram. Soc., **69** [6] 499-506 (1986).

5. M. N. Rahaman and L. C. De Jonghe, *"Creep-Sintering of ZnO,"* J. Mater. Sci., **22** 4326-4330 (1987).

6. M-Y. Chu, L. C. De Jonghe, and M. N. Rahaman, *"Effect of Temperature on the Densification/Creep Viscosity During Sintering,"* Acta metall., **37** [5] 1415-1420 (1989).

7. L. C. De Jonghe and M. N. Rahaman, *"Sintering Stress of Homogeneous and Heterogeneous Powder Compacts,"* Acta Metall., **36** [1] 223-229 (1988).

8. C. A. Bruch, *"Sintering Kinetics for the High Density Alumina Process,"* Am. Ceram. Soc. Bull., **41** [12] 799-806 (1962).

9. C. Greskovich, *"Effect of Green Density on the Initial Sintering of Alumina,"* Physics of Sintering, **4** [1] 33-46 (1972).

10. J. L. Woolfrey, *"Effect of Green Density on the Initial-Stage Sintering Kinetics of UO2,"* J. Am. Ceram. Soc., **55** [8] 383-389 (1972).

11. M. A. Occhionero and J. W. Halloran, *"The Influence of Green Density on Sintering,"* pp. 89-102 in Sintering and Heterogeneous Catalysis (Materials

Science Research; Vol. 16). Edited by G. C. Kuczynski, A. E. Miller, and G. A. Gordon. Plenum Press, New York, 1984.

12. M. F. Yan, R. M. Cannon and U. Chowdhry, *"Theory of Grain Growth During Densification,"* discussed in M. F. Yan, Mater. Sci. Engr., **48** [1] 53-72 (1981).

13. W. Beere, *"A Unifying Theory of the Stability of Penetrating Liquid Phases and Sintering Pores,"* Act metall., **23** [1] 131-138 (1975).

14. W. Beere, *"The Second Stage Sintering Kinetics of Powder Compacts,"* Acta metall., **23** [1] 139-145 (1975).

15. F. R. N. Nabarro, *"Deformation of Crystals by the Motion of Single Ions,"* p. 75-90 in Report on e Conference of Strength of Solids, Bristol, England, 1947, 1948.

16. C. Herring, *"Diffusional Viscosity of a Polycrystalline Solid,"* J. Appl. Phys., **21** [5] 437-445 (1950).

17. R. L. Coble, *"A Model for Boundary Diffusion Controlled Creep in Polycrystalline Materials,"* J. Appl. Phys., **34** [6] 1679-1682 (1963).

18. B. J. Kellett and F. F. Lang, *"Thermodynamics of Densification: I, Sintering Simple Particle Arrays, Equilibrium Configuration, Pore Stability, and Shrinkage"*, J. Am. Ceram. Soc., **12** [5], 725-34 (1989).

19. T. K. Gupta and R. L. Coble, *"Sintering of ZnO: I, Densification and Grain Growth,"* J. Am. Ceram. Soc., **51** [9] 521-525 (1968).

20. M-Y. Chu, M. N. Rahaman, and L. C. De Jonghe, *"The Effect of Heating Rate on Sintering and Coarsening,"* unpublished work (LBL report #26823, 1989).

21. G. G. Long, S. Krueger, and R. A. Page, *"Processing - Microstructure Relations During Sintering of Alumina and Porous Silica"*, paper presented at the 92nd Annual Meeing, Amer. Ceram. Soc., Dallas, 1990, paper number 108-SV-90.

Figure Captions

Fig. 1. Axial strain versus temperature for ZnO powder compacts with different green densities that were sintered freely or with an applied uniaxial stress, σ_Z, of 0.22 MPa. Data for sample green densities of 0.51 and 0.66 have been omitted in order to maintain clarity. The samples were heated in air at 4°C/min to 1100°C.

Fig. 2. Axial strain versus radial strain for the samples described in Fig. 1 that were sintered under a uniaxial stress.

Fig. 3. Relative density versus temperature for the samples described in Fig. 1 that were sintered freely.

Fig. 4. Densification rate versus temperature calculated from the density data of Fig. 3.

Fig. 5. Densification rate versus sintered density calculated from the data of Fig. 3.

Fig. 6. Creep rate versus sintered density calculated from the data of Figs. 1 and 2 for the samples sintered under a uniaxial stress.

Fig. 7. Ratio of the densification rate to the creep rate versus temperature for the samples described in Fig. 1. The creep rate has been normalized at a constant uniaxial stress of 0.20 MPa.

Fig. 8. Scanning electron micrographs of the fracture surfaces of samples with green densities of (a) 0.39, (b) 0.51, and (c) 0.73, that were sintered at a heating rate of 4°C/min to 1100°C.

Fig. 9. Scanning electron micrographs of the fracture surfaces of samples with green densities of (a) 0.39 and (b) 0.73 that were sintered at a heating rate of 4°C/min to a relative density of 0.81.

Fig. 10. Ratio of the densification rate to the constant stress creep rate (at a fixed temperature of 650°C) versus green density.

Fig. 11. The coarsening function, X^n, versus sintered density computed from Eqns. (3), (4) and (8) and the data of Figs. 3 and 4 for green densities between 0.39 and 0.73.

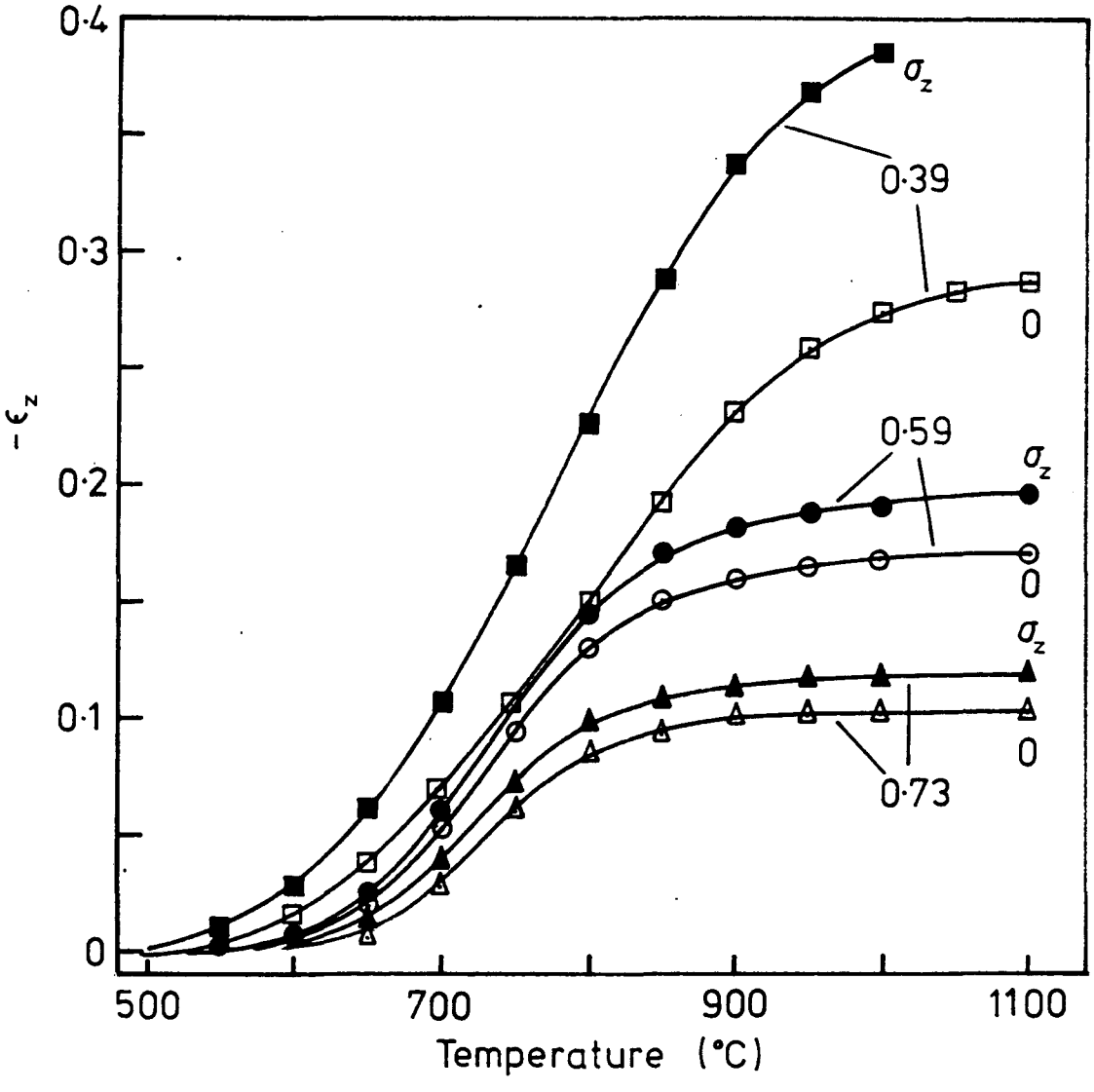
0·4
0·3
0·2
0·1
0
$-\varepsilon_z$
500
700
900
1100
Temperature (°C)
σ_z
0·39
0
0·59
σ_z
0
σ_z
0
0·73
XBL 903-912

Figure 1

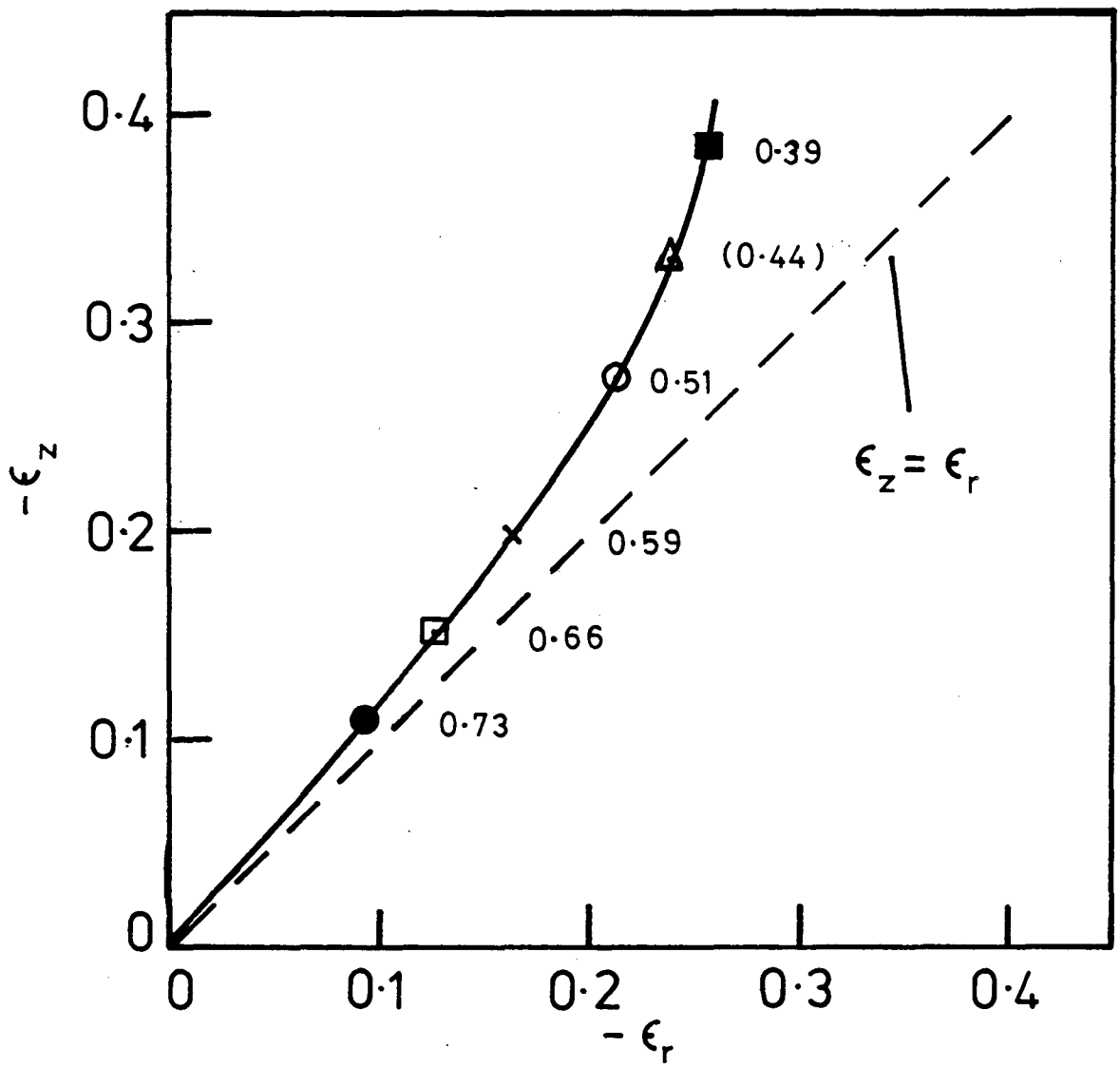

XBL 903-913

Figure 2

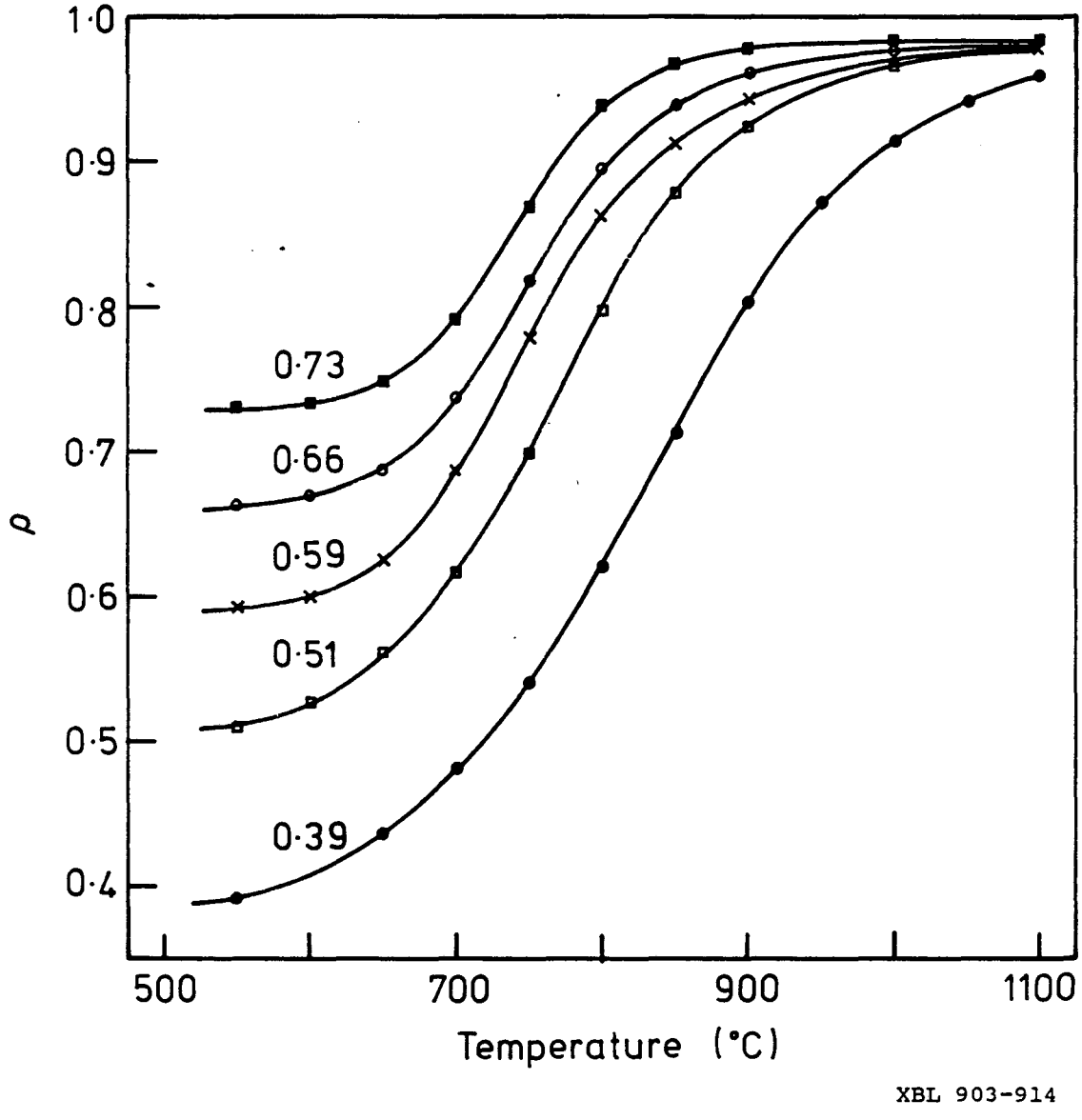
1·0
0·9
0·8
0·7
0·6
0·5
0·4
ρ
0·73
0·66
0·59
0·51
0·39
500
700
900
1100
Temperature (°C)
XBL 903-914

Figure 3

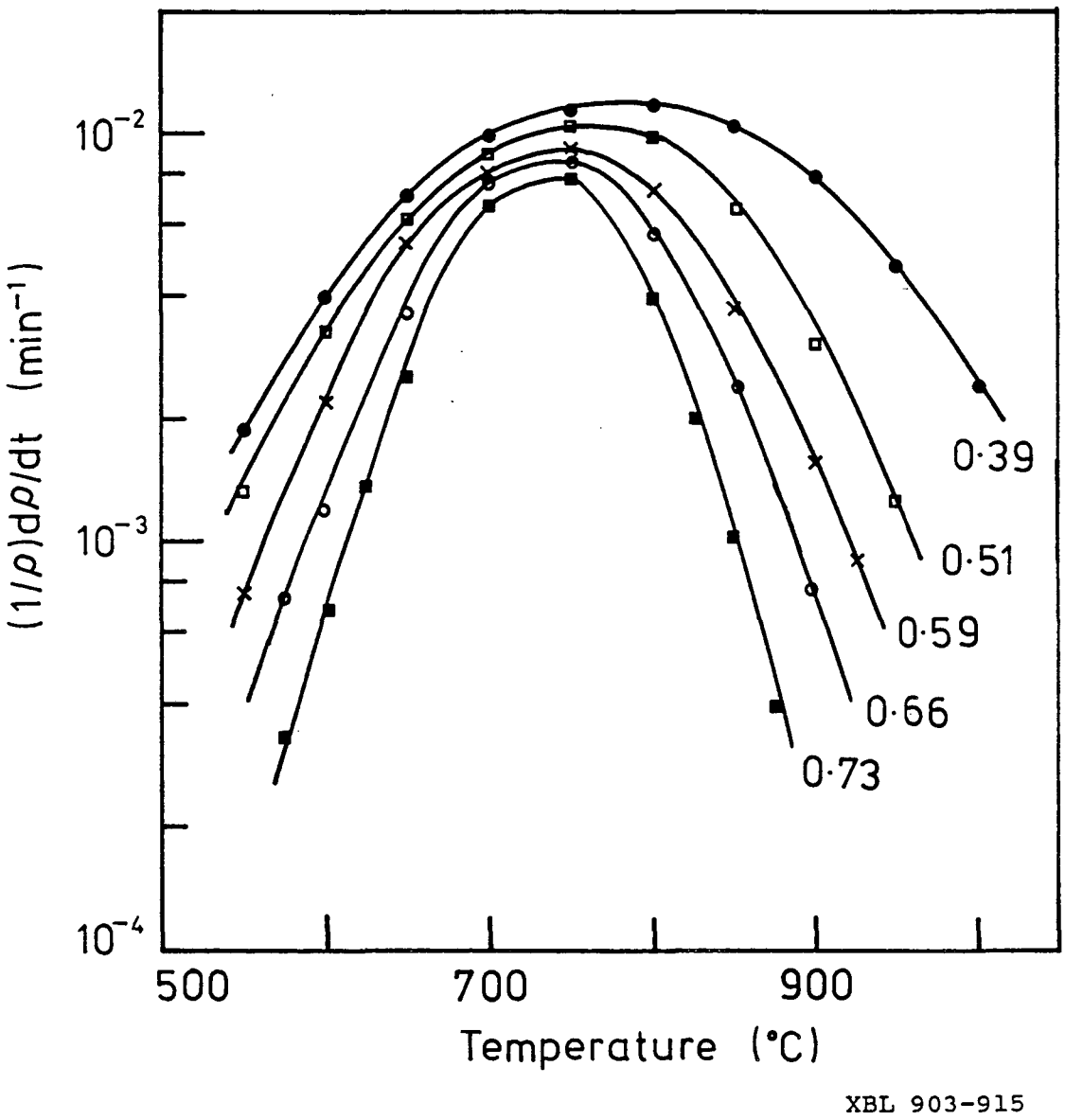
10^{-2}
10^{-3}
10^{-4}
$(1/\rho)d\rho/dt$ (min^{-1})
0·39
0·51
0·59
0·66
0·73
500
700
900
Temperature (°C)
XBL 903-915

Figure 4

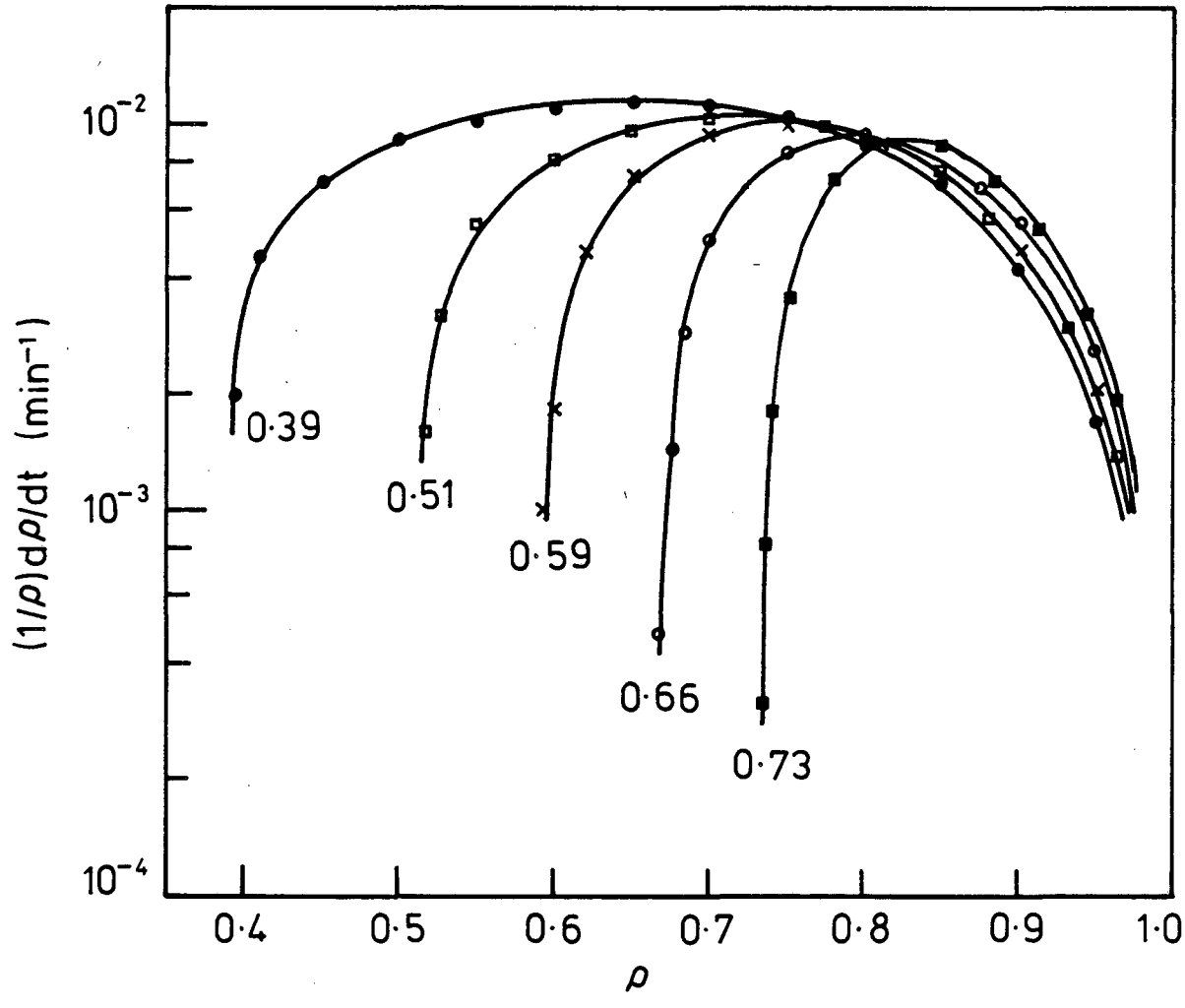
10^{-2}
10^{-3}
10^{-4}
$(1/\rho)d\rho/dt$ (min^{-1})
0·39
0·51
0·59
0·66
0·73
0·4
0·5
0·6
0·7
0·8
0·9
1·0
ρ
XBL 903-916

Figure 5

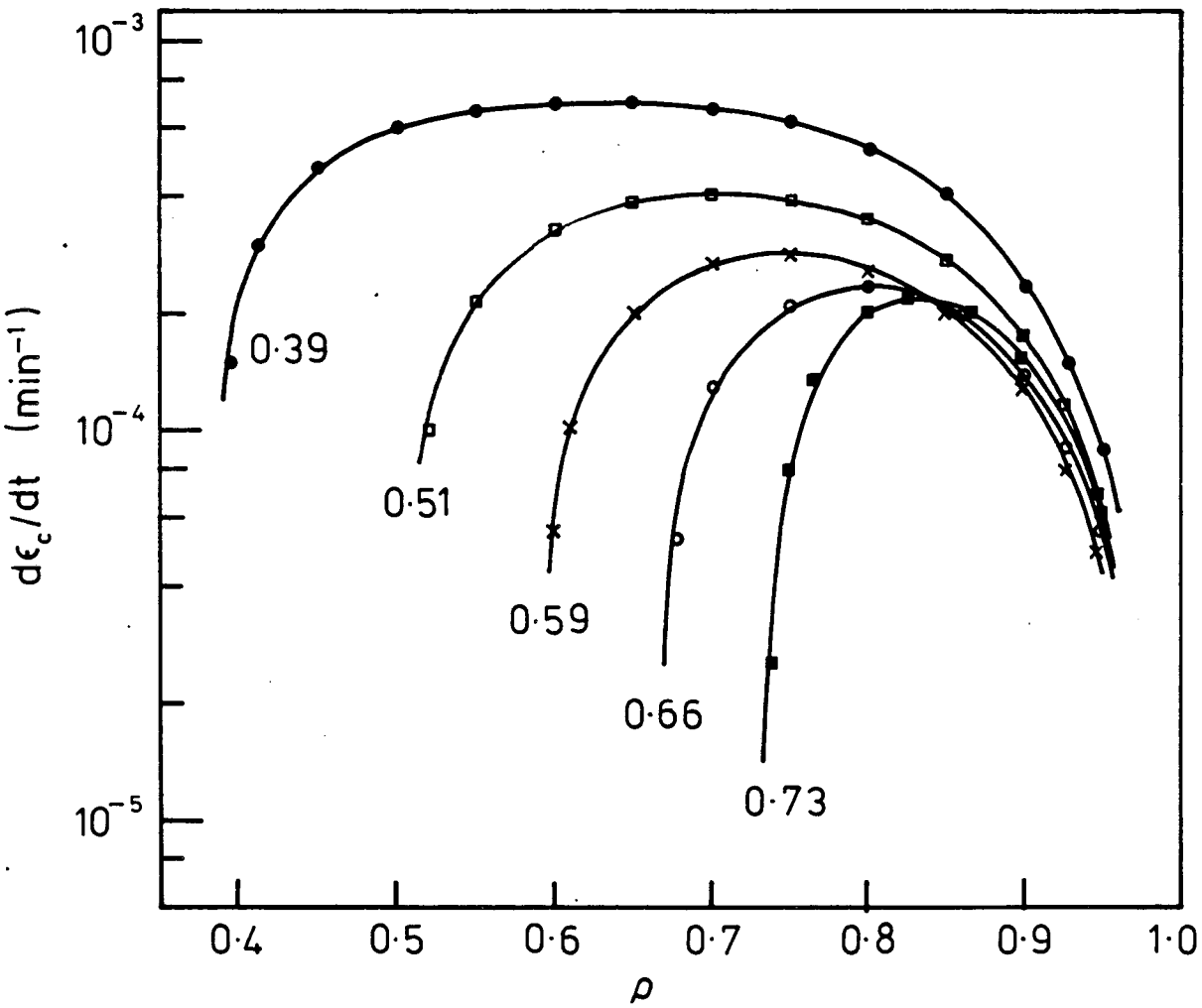
10^{-3}
10^{-4}
10^{-5}
$d\epsilon_c/dt$ (min^{-1})
0·39
0·51
0·59
0·66
0·73
0·4
0·5
0·6
0·7
0·8
0·9
1·0
ρ
XBL 903-917

Figure 6

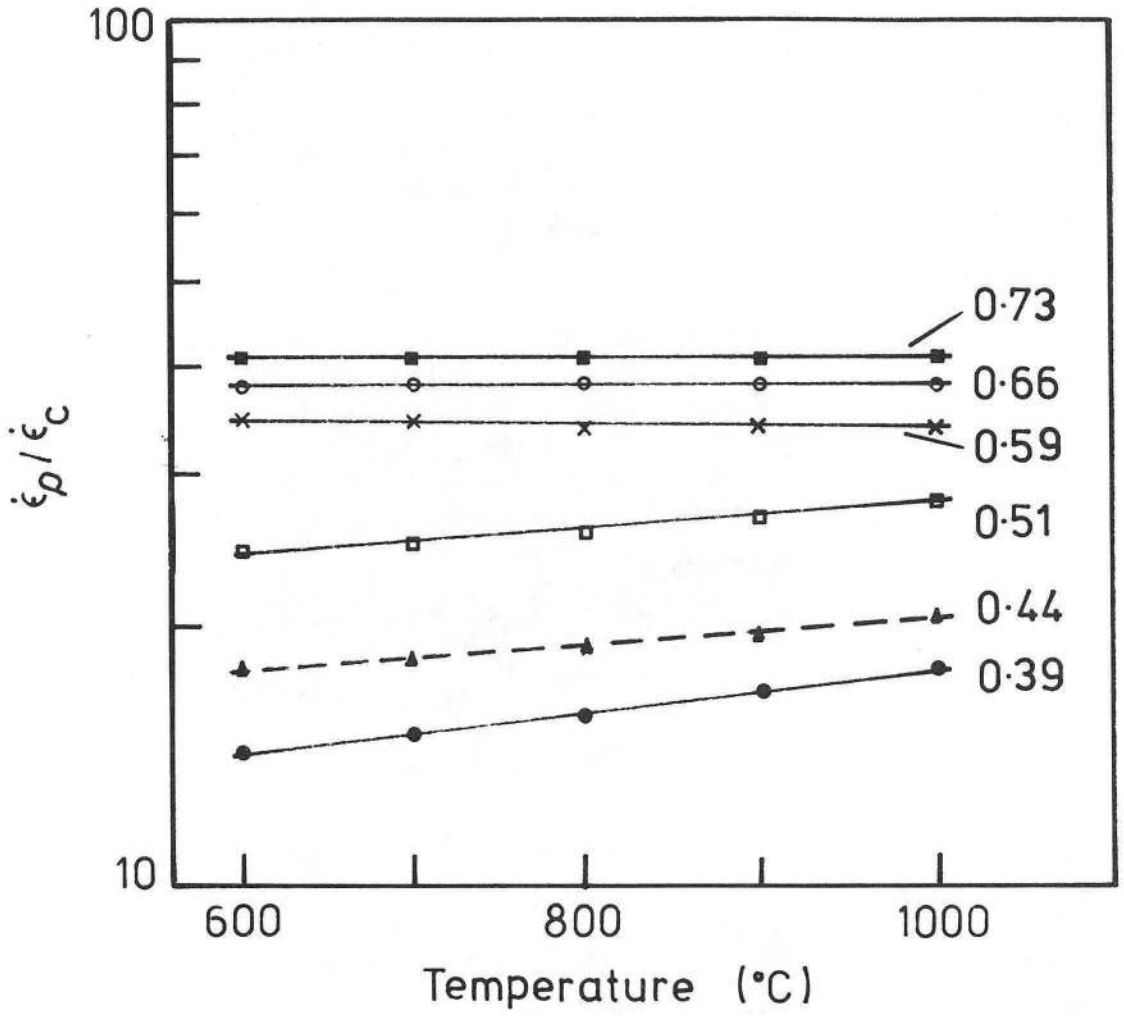
100
10
600
800
1000
Temperature (°C)
$\dot{\epsilon}_p/\dot{\epsilon}_c$
0·73
0·66
0·59
0·51
0·44
0·39
XBL 903-918

Figure 7

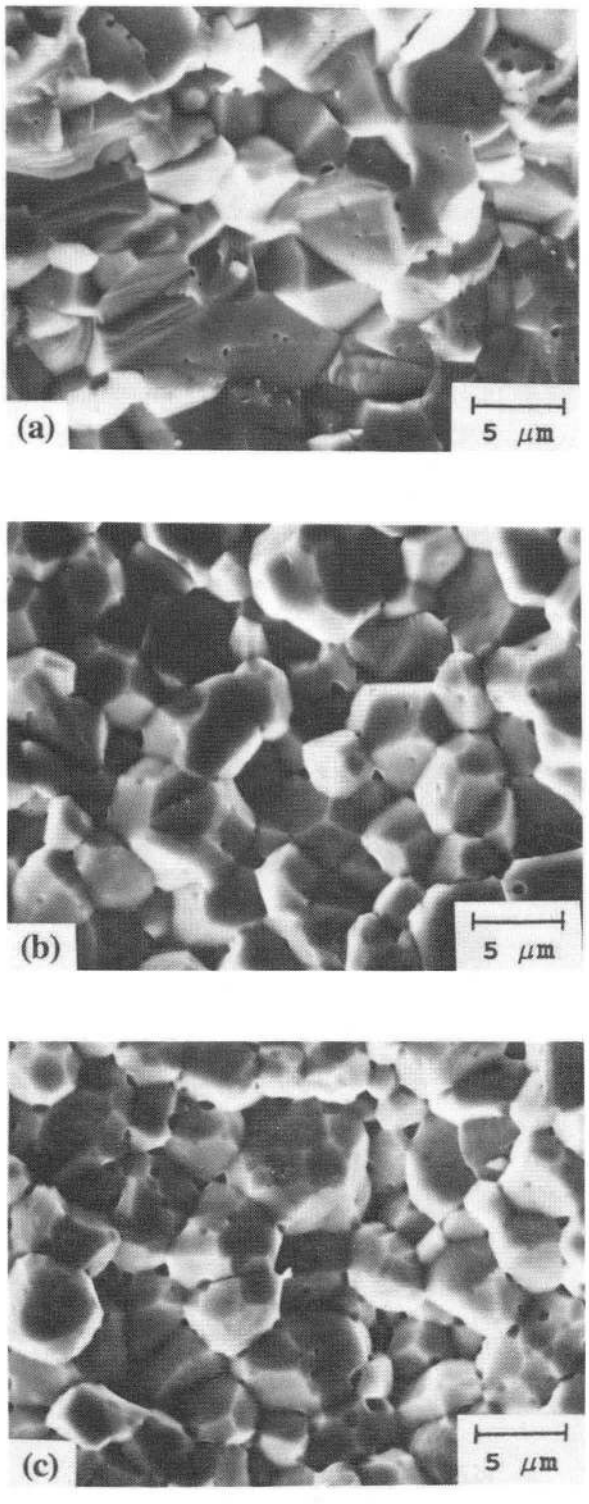

XBB 903 – 1957

Figure 8

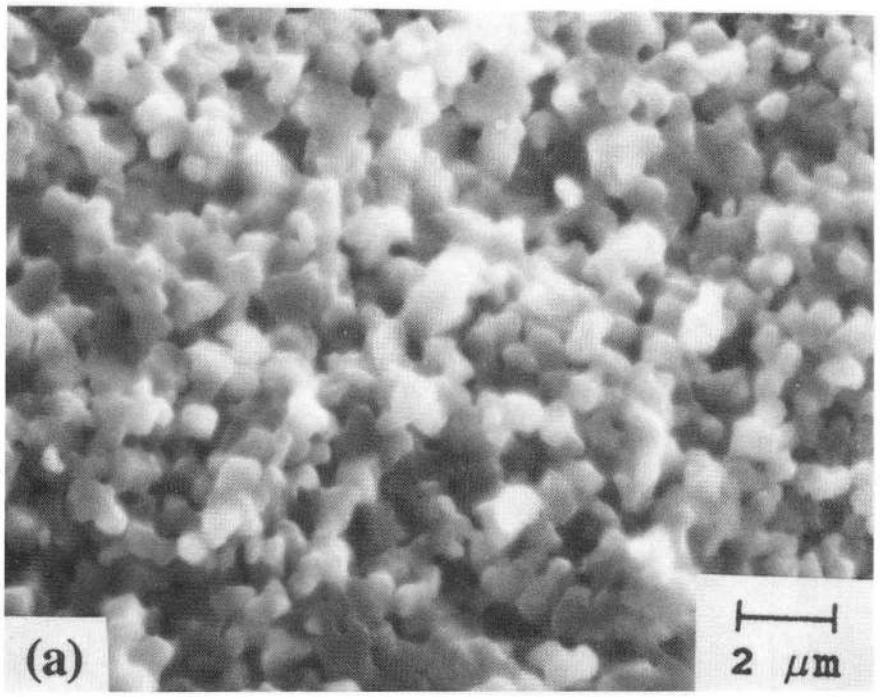

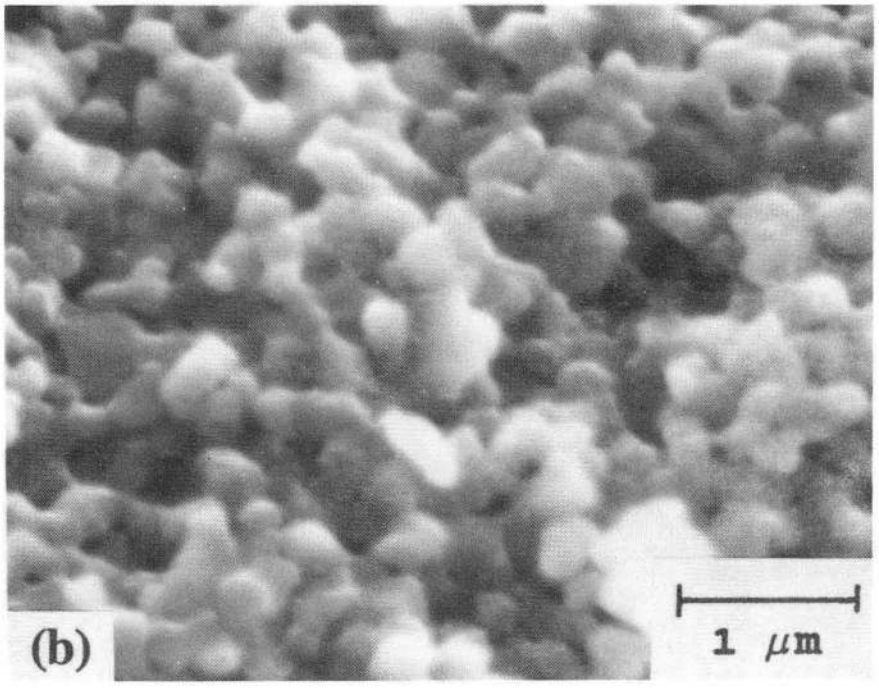

XBB 903 – 1958

Figure 9

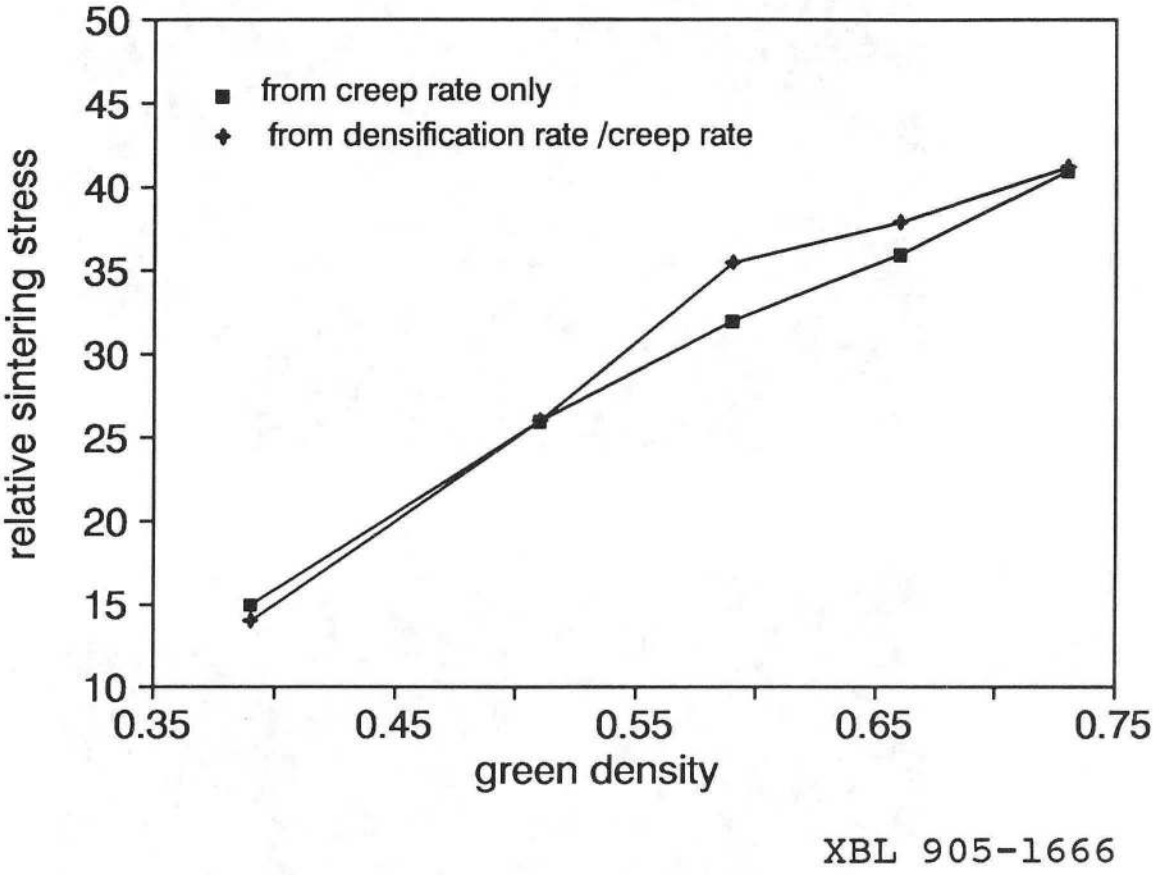
50
45
40
35
30
25
20
15
10
relative sintering stress
from creep rate only
from densification rate /creep rate
0.35
0.45
0.55
0.65
0.75
green density
XBL 905-1666

Figure 10

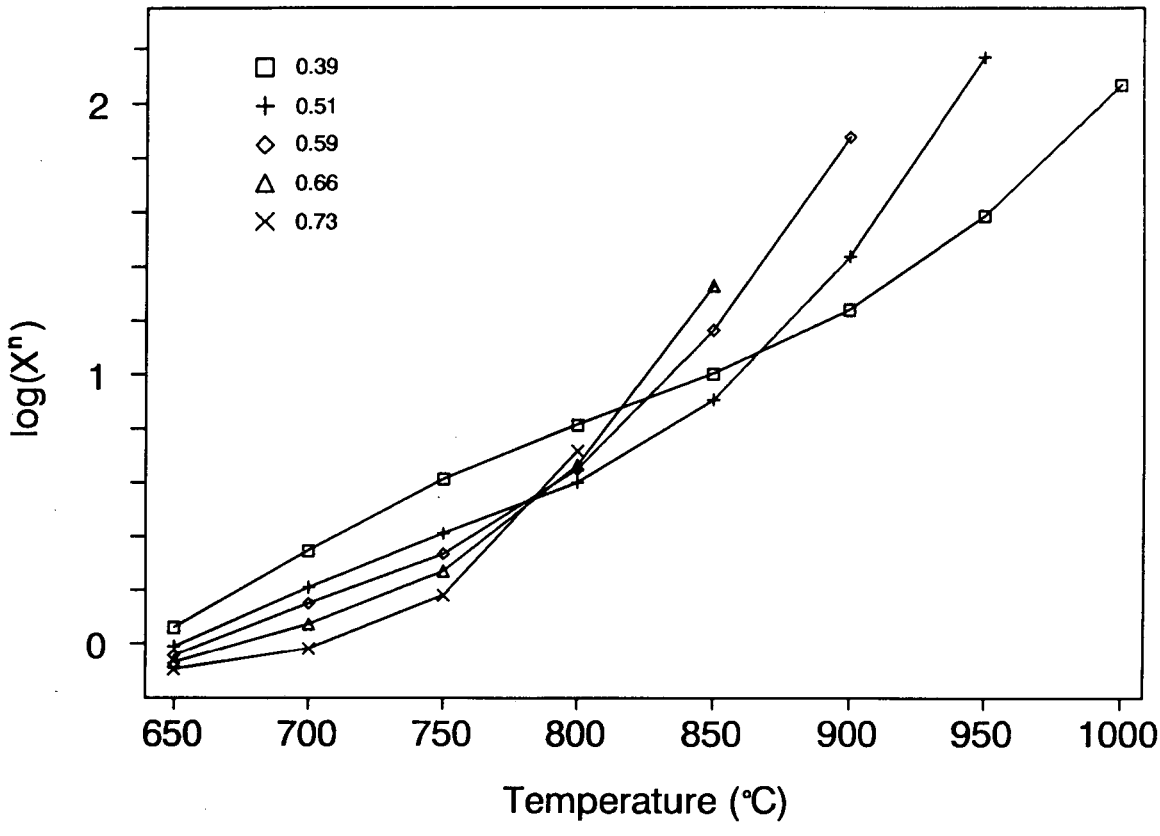

XBL 905-1665

Figure 11

LAWRENCE BERKELEY LABORATORY
UNIVERSITY OF CALIFORNIA
INFORMATION RESOURCES DEPARTMENT
BERKELEY, CALIFORNIA 94720